The EMBO Journal Vol. 21 No. 19 pp. 5057–5068, 2002

Binding of the PX domain of p47^{phox} to phosphatidylinositol 3,4-bisphosphate and phosphatidic acid is masked by an intramolecular interaction

Dimitrios Karathanassis[1], Robert V.Stahelin[2], Jerónimo Bravo[1,3], Olga Perisic[1], Christine M.Pacold[1], Wonhwa Cho[2] and Roger L.Williams[1,4]

[1]MRC Laboratory of Molecular Biology, Hills Road, Cambridge CB2 2QH, UK and [2]Department of Chemistry, University of Illinois at Chicago, Chicago, IL 60607, USA

[3]Present address: Structural Biology Program, Centro Nacional de Investigaciones Oncológicas, Melchor Fernández Almagro 3, E-28029 Madrid, Spain

[4]Corresponding author
e-mail: rlw@mrc-lmb.cam.ac.uk

p47^{phox} is a key cytosolic subunit required for activation of phagocyte NADPH oxidase. The X-ray structure of the p47^{phox} PX domain revealed two distinct basic pockets on the membrane-binding surface, each occupied by a sulfate. These two pockets have different specificities: one preferentially binds phosphatidylinositol 3,4-bisphosphate [PtdIns(3,4)P_2] and is analogous to the phophatidylinositol 3-phosphate (PtdIns3P)-binding pocket of p40^{phox}, while the other binds anionic phospholipids such as phosphatidic acid (PtdOH) or phosphatidylserine. The preference of this second site for PtdOH may be related to previously observed activation of NADPH oxidase by PtdOH. Simultaneous occupancy of the two phospholipid-binding pockets radically increases membrane affinity. Strikingly, measurements for full-length p47^{phox} show that membrane interaction by the PX domain is masked by an intramolecular association with the C-terminal SH3 domain (C-SH3). Either a site-specific mutation in C-SH3 (W263R) or a mimic of the phosphorylated form of p47^{phox} [Ser(303, 304, 328, 359, 370)Glu] cause a transition from a closed to an open conformation that binds membranes with a greater affinity than the isolated PX domain.

Keywords: NADPH oxidase/p40/phagocyte/phosphatidic acid/phosphoinositide/SH3 domains

Introduction

NADPH oxidase plays a decisive role in the ability of phagocytes to defend against bacterial infections. The enzyme catalyses the transfer of an electron from NADPH to oxygen to form superoxide that acts as a precursor to microbicidal oxidants. The NADPH oxidase activity also results in release of proteases within the phagosome (Reeves *et al*., 2002). The phagocyte oxidase consists of a membrane-bound, catalytic gp91^{phox}–p22^{phox} heterodimer known as flavocytochrome b_{558}, and cytosolic regulatory subunits consisting of p40^{phox}, p47^{phox}, p67^{phox} and Rac (reviewed in Babior, 1999). p40^{phox}, p47^{phox} and p67^{phox} form a 1:1:1 complex in the resting state (Lapouge *et al*., 2002). Because of the potentially damaging reactions that can be initiated by the oxidase, the enzymatic activity is tightly regulated. Electron microscopy studies show that gp91^{phox} and p22^{phox} are located in the membranes of specific granules, gelatinase granules and secretory vesicles (reviewed in Seguchi and Kobayashi, 2002). Activation of the oxidase requires translocation of the cytosolic subunits to the membrane-bound flavocytochrome, yet the mechanism of this translocation is not clear. The p47^{phox} subunit appears to have a key role in translocation. Studies of cells from chronic granulomatous disease (CGD) patients deficient in p47^{phox} indicate that this subunit is required for translocation of p40^{phox} and p67^{phox} (Heyworth *et al*., 1991; Uhlinger *et al*., 1993; Dusi *et al*., 1996). Translocation of the cytosolic subunits to membranes could be the consequence of direct membrane interactions or interactions with membrane-localized proteins. Interaction between p47^{phox} and the intrinsic membrane protein p22^{phox} may play a role in translocating p47^{phox}. Other interactions between NADPH oxidase cytosolic subunits and membrane-interacting proteins have been reported, but the significance of these for the activation of NADPH oxidase is not yet clear, e.g. both p47^{phox} and p40^{phox} interact with moesin, a protein with both membrane- and actin-binding domains (Wientjes *et al*., 2001), and p67^{phox} interacts with JFC1, a protein that has a 3-phosphoinositide-binding domain (McAdara Berkowitz *et al*., 2001).

Recently, it was shown that both p47^{phox} and p40^{phox} can interact directly with membranes via their N-terminal PX domains (Ago *et al*., 2001; Ellson *et al*., 2001; Kanai *et al*., 2001). These direct membrane interactions may play a role in translocation, or they may be important for activation of the NADPH oxidase once the cytosolic subunits have already associated with the membrane. The PX domain of p47^{phox} preferentially binds to vesicles containing phosphatidylinositol 3,4-bisphosphate [PtdIns(3,4)P_2] (Kanai *et al*., 2001), whereas the p40^{phox}-PX, like most other PX domains, has a strong preference for phosphatidylinositol 3-phosphate (PtdIns3P) (Ellson *et al*., 2001; Kanai *et al*., 2001; Yu and Lemmon, 2001). Binding of PtdIns3P to p40^{phox}-PX stimulates NADPH oxidase activity *in vitro* (Ellson *et al*., 2001). We previously reported the structure of the p40^{phox} PX domain in a complex with PtdIns3P (Bravo *et al*., 2001); however, the lipid-binding pocket in this structure was very different from the analogous pocket in the NMR structure of the p47^{phox}-PX (Hiroaki *et al*., 2001). We report here a high-resolution X-ray structure of the p47^{phox} PX domain showing two basic pockets occupied by sulfates that represent two potential phospholipid-binding sites. Using structure-guided mutagenesis and phospholipid-binding measurements, we show that these two sites strongly synergize in membrane

Table I. Data collection, structure determination and refinement statistics

Data collection and MAD phasing statistics Data set	Peak[c]	Inflection[c]
Resolution (Å)	2.0	2.0
Observations/unique reflections	83 922/24 307	84 280/24 356
Completeness (last shell) %	93.6 (74.1)	93.7 (74.1)
R_{merge}[a]	0.050	0.044
$\langle I/\sigma \rangle$ (last shell)	20.1 (1.5)	19.7 (1.3)
Phasing power (iso)[b]	–	0.74
Phasing power (anom)[b]	2.1	1.3
Refinement statistics		
Resolution (Å)	38.9–2.0	
Protein atoms	3018	
Heterogen atoms	35	
Water molecules	204	
R_{cryst}[d]	0.22	
R_{free}[d] (% data used)	0.27 (5.0)	
R.m.s.d. from ideality[e]		
Bonds	0.020 Å	
Angles	1.7°	
Dihedrals	25°	

Overall figure of merit 0.43 before solvent flattening and 0.88 after solvent flattening.
[a]$R_{merge} = \Sigma_{hkl}\Sigma_i |I_i(hkl) - \langle I(hkl)\rangle| / \Sigma_{hkl}\Sigma_i I_i(hkl)$
[b]The phasing power is defined as the ratio of the r.m.s. value of the heavy atom structure factor amplitudes to the r.m.s. value of the lack-of-closure error.
[c]Data sets were collected at ESRF beamline ID29.
[d]R_{cryst} and $R_{free} = \Sigma |F_{obs} - F_{calc}| / \Sigma F_{obs}$; R_{free} calculated with the percentage of the data shown in parentheses.
[e]R.m.s. deviations for bond angles and lengths with regard to Engh and Huber parameters.

binding. In the context of the full-length p47*phox*, membrane binding by both sites is masked by intramolecular interaction with the C-terminal SH3 domain (C-SH3) and unmasked in a phosphorylation mimic.

Results

Description of the overall structure

The X-ray structure of the p47*phox* PX domain was determined at 2.0 Å resolution by multiple anomalous dispersion (MAD) techniques for a crystal of selenomethionine-substituted protein (Table I). The overall fold consists of a three-stranded antiparallel β-sheet followed by a helical subdomain containing four α-helices and a polyproline II region (Figure 1). There are two sulfates bound on the same surface of the domain. One sulfate is in a basic pocket with a location analogous to the PtdIns3P-binding pocket of p40*phox*-PX (Bravo *et al.*, 2001). The second sulfate is bound in a distinct shallow pocket that has no analogue in previously characterized PX domains (Figure 1).

The C_α positions of the p47*phox* and p40*phox* PX domains closely superimpose throughout the domain except in the region from 59 to 86 (p47*phox* numbering) containing helix α1′, a distorted, left-handed PP_{II} helix and the succeeding membrane insertion loop (residues 77–86). This 59–86 region also deviates greatly from what was observed in the NMR study of the p47*phox*-PX (Hiroaki *et al.*, 2001). However, because part of this region forms much of the contact area between molecules in the asymmetric unit,

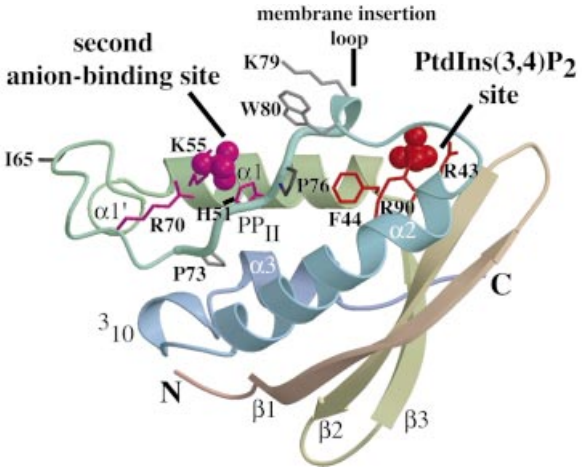

Fig. 1. The structure of the p47*phox* PX domain. The ribbon representation is coloured from red at the N-terminus to blue at the C-terminus. Selected residues are shown in stick representation. Residues in the phosphoinositide pocket are shown in red and those lining the second anion-binding pocket are coloured magenta. The sulfates bound in the two pockets are shown in CPK representation.

some of these differences may arise due to crystal contacts. The membrane insertion loop is important for the shape of the phosphoinositide-binding pocket. Unlike the recently reported NMR structure of the unliganded Vam7p-PX, which has a PtdIns3P-binding pocket nearly identical to the p40*phox*-PX (Lu *et al.*, 2002), the p47*phox*-PX has a phosphoinositide-binding pocket with considerable conformational differences. This conformational variation in the membrane insertion loop is not surprising given the sequence variation among PX domains in this region.

The structure of the phosphoinositide-binding pocket

Superimposing the p40*phox* PX domain on p47*phox* shows that the sulfate in the p47*phox* phosphoinositide-binding pocket is at the position of the 3-phosphate of the phosphoinositide bound to the p40*phox*-PX (Figure 2). The sulfate is hydrogen bonded to Arg43 and is within van der Waals contact distance of Arg90 (Figure 3). These two residues are equivalent to Arg58 and Arg105 of the p40*phox* PX domain, which are critical for PtdIns3P binding to the p40*phox*-PX and interact with the 3-phosphate and 4- and 5-OH groups, respectively. The most striking feature of the p47*phox*-PX phosphoinositide-binding pocket in comparison with p40*phox*-PX is the wide crevice between the C-terminal end of β2 and the N-terminal end of α2 (Figure 4).

Within the p47*phox*-PX PtdIns(3,4)P_2-binding site, Arg43 [the middle residue of the conserved (R/K)-(R/K)-(F/Y) motif located in the β3/α1 loop] superimposes closely with p40*phox* Arg58 and presumably has the same role as the principal 3-phosphate ligand (Figure 2). Arg90 (in the α2 helix) superimposes with p40*phox* Arg105 and, by analogy with p40*phox*, would be best placed to act as the ligand of the 4- and 5-positions of the phosphoinositide. However, if PtdIns(3,4)P_2 were placed in the p47*phox* pocket in the same orientation as the PtdIns3P in p40*phox*, there would be a few steric clashes caused by differences in the shapes of the pockets. First, there is no room to accommodate the 4-phosphate because

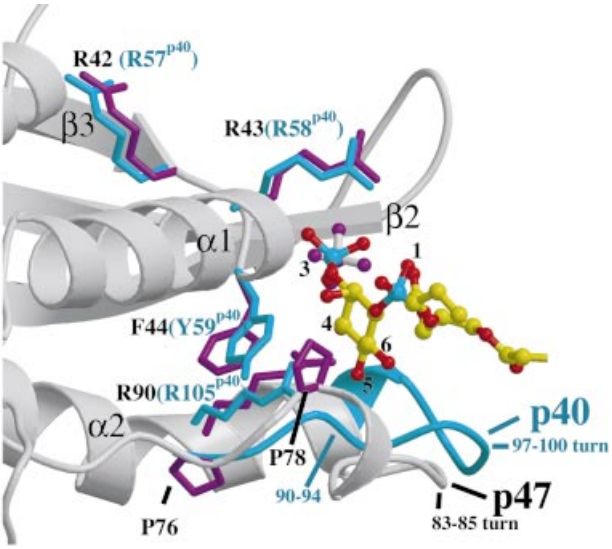

Fig. 2. A comparison of the phosphoinositide-binding pockets of the p47^{phox} and p40^{phox} PX domains. The C_α atoms of the two domains were superimposed. The p47^{phox}-PX is shown as a grey ribbon, while for p40^{phox} the main chain ribbon (cyan) is shown only in the region of the phosphoinositide-binding pocket where the structures differ greatly. The side chains of residues that are critical for phosphoinositide binding are shown, with residue numbers for p40^{phox} in parentheses. The side chain of Pro78 that protrudes into the binding pocket in p47^{phox} is also illustrated. The bound PtdIns3P from the p40^{phox}-PX structure is also shown (coloured yellow, red and cyan for carbon, oxygen and phosphorus, respectively). The sulfate in the phosphoinositide-binding pocket of p47^{phox}-PX (grey bonds and magenta atoms) coincides with the location of the 3-phosphate of PtdIns3P. Arg42 that is associated with a CGD mutation points away from the binding site and has a role in stabilizing p47^{phox} (Heyworth and Cross, 2002).

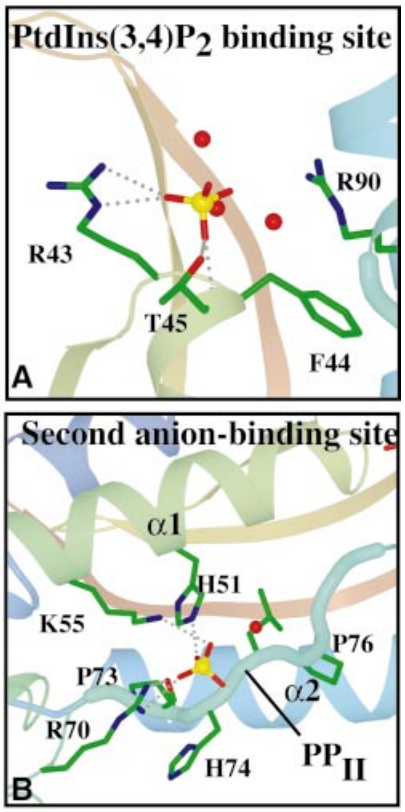

Fig. 3. Interactions with the sulfates bound in the phosphoinositide-binding and second anion-binding pockets of p47^{phox}-PX. Dashed lines represent hydrogen bonding interactions with the protein. Ordered waters associated with the sulfates are shown as red spheres.

of the proximity of Arg90. Secondly, part of the pocket that binds PtdIns3P in p40^{phox} is sterically hindered by the Pro78 side chain because the main chain of the region from 78 to 80 adopts a short 3_{10} helix as opposed to the extended conformation of the analogous region, 90–94, in p40^{phox} (Figures 2 and 4). In p47^{phox}, Pro78 covers most of the Phe44 side chain. The residue analogous to Phe44 in p40^{phox} (Tyr59) is essential for phospholipid binding and contacts one face of the inositide ring, suggesting either that phosphoinositides bind somewhat differently to these two PX domains or that binding to p47^{phox} is accompanied by a conformational change that removes the occlusion imposed by Pro78. Given the steric clashes presented by both Arg90 and the 78–80 turn, it is most likely that the PtdIns(3,4)P_2 headgroup would be rotated in the binding pocket so that the 3- and 4-phosphates interact with Arg43 and Arg90, respectively, and that the inositide ring would be shifted into the crevice created between the ends of β2 and α2 (Figure 4C). This crevice provides additional space that could accommodate the alternative phosphoinositide orientation in the p47^{phox}-binding pocket relative to p40^{phox} and is created by the very different conformation of the p47^{phox} 83–85 turn. In the p40^{phox} pocket, the analogous region (97–100) folds into the pocket and closes the crevice (Figure 4).

The structure of the second anion-binding pocket

Besides the bound sulfate in the putative phosphoinositide-binding pocket, the structure revealed another sulfate bound in a separate, shallower basic pocket. This secondary pocket is on the same surface of the domain as the phosphoinositide-binding pocket and is separated from it by a ridge made up of the membrane insertion loop (Figures 1 and 4). Walls of this pocket are formed by the side chains of Arg70, Lys55 and His51, giving it a basic character. The guanidinium group of Arg70 forms an extensive set of hydrogen bonding interactions both with the bound sulfate and with the backbone of Pro73 in the polyproline helix of the conserved PXXP motif (residues 73–76, Figures 1 and 3). The second anion-binding site is not present in either of the two PX domains whose structures were determined previously, p40^{phox}-PX and Vam7p-PX. The presence of two basic residues analogous to Arg70 and Lys55 is an unusual feature among PX domain sequences, and only the PX domains from p47^{phox} and phospholipase D (PLD) appear to have such a feature (Figure 5).

Arg70 is part of an (R/K)XXPXXP sequence motif that has been defined as a type I SH3-interacting motif (Mayer, 2001). A small subset of PX domains (besides p47^{phox} and PLD) contain this motif, including the PX domains of the mammalian proteins FISH and sorting nexin 8, and the yeast proteins Mvp1 and Bem1, suggesting that these PX domains may, like p47^{phox}-PX, bind to SH3 domains. In structures of complexes of SH3 domains with type I motif-containing peptides, the basic residue of the motif uses its side chain to interact with the negatively charged specificity pocket of the SH3 domain (Mayer, 2001), and the C_δ atoms of the prolines from the PXXP motif occupy

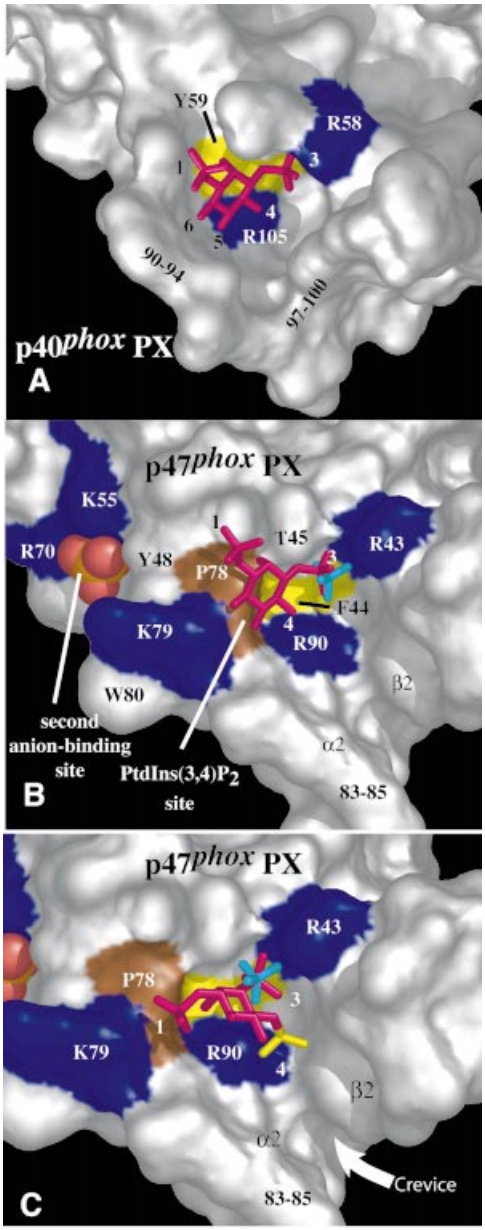

Fig. 4. Solid representations of the p40*phox* and p47*phox* PX domains. (**A**) View of the PtdIns3P (magenta) bound to the p40*phox*-PX. The principal ligands of the phosphoinositide, Arg58 and Arg105, are highlighted in blue, and Tyr59 at the bottom of the pocket is shown in yellow. (**B**) View of the membrane-binding surface of the p47*phox*-PX showing both phospholipid-binding sites with basic residues highlighted in blue. The sulfate in the phosphoinositide-binding site is shown in stick representation (coloured cyan). PtdIns3P from the superimposed structure of the p40*phox*-PX is illustrated (stick representation). The 3-phosphate of the PtdIns3P coincides with the bound sulfate in the p47*phox* phosphoinositide pocket. The Pro78 that sterically clashes with the PtdIns3P is highlighted in brown. The sulfate in the second anion-binding site is shown in CPK representation (coloured red and brown). (**C**) A model of a PtdIns(3,4)P_2 bound in the p47*phox*-PX phosphoinositide-binding pocket. To avoid steric clashes, the inositide ring has been rotated ~90° while maintaining the 3- and 4-phosphates in contact with the side chains of Arg43 and Arg90, respectively. The 4-phosphate (yellow) is extending into the crevice between β2 and α2. This crevice is filled by residues 97–100 in p40*phox* [as seen in (A)].

adjacent hydrophobic pockets on the surface of the SH3 domain. In p47*phox*, only one proline (Pro76) from the PXXP motif is accessible for interaction, while the other (Pro73) is buried (Hiroaki *et al*., 2001; and Figure 1). In addition, the Arg70–Pro73 backbone interaction that we see in p47*phox* would preclude Arg70 binding in an SH3 domain specificity pocket. These observations suggest that if the proline-rich region of the p47*phox*-PX were to interact with the C-SH3 in a typical manner, p47*phox*-PX would have to undergo a conformational change.

Phosphoinositide specificity of the p47phox PX domain

In order to determine the roles of the two apparent phospholipid-binding sites suggested by the structure and to elucidate the mechanism of membrane binding, we measured the vesicle binding of wild-type and a series of site-specific mutants by surface plasmon resonance (SPR) and sedimentation measurements.

We first measured the binding of wild-type p47*phox*-PX to various phosphoinositide-containing lipid vesicles immobilized to the sensor surface by kinetic SPR analysis to determine the effects of phosphoinositides on membrane binding of p47*phox*-PX. In the absence of phosphoinositide, p47*phox*-PX has extremely low affinity for 1-palmitoyl-2-oleoyl-*sn*-glycero-3-phosphocholine (POPC)/1-palmitoyl-2-oleoyl-*sn*-glycero-phosphoethanolamine (POPE) (80:20) vesicles (K_d >20 μM). Increasing the concentration of PtdIns(3,4)P_2 in the vesicles from 0 to 3% dramatically increases the affinity (K_d = 38 nM) (Table II). To validate the K_d value determined from the kinetic SPR analysis, we also determined the K_d for p47*phox*-PX by equilibrium SPR analysis and by a sedimentation assay using lipid-coated beads (Kim *et al*., 1997) and radiolabelled PX domain. As shown in Figure 6, the K_d values (38 ± 0.1 and 30 ± 7 nM) calculated from the equilibrium binding isotherms agree well with the K_d determined from the kinetic analysis. Table II shows that p47*phox*-PX has 18- to 26-fold greater affinity for PtdIns(3,4)P_2 than for any other tested phosphoinositide, confirming the reported specificity of the p47*phox*-PX for PtdIns(3,4)P_2 (Kanai *et al*., 2001).

The enhanced membrane affinity of the p47*phox*-PX domain due to 3 mol% PtdIns(3,4)P_2 is almost entirely due to a decrease in the k_d, with the k_a remaining nearly constant. This is consistent with our previous finding that short-range specific interactions increase membrane affinity mainly by decreasing the k_d (Stahelin and Cho, 2001). The only other phosphoinositide-binding domain known to bind specifically PtdIns(3,4)P_2 is the C-terminal PH domain of TAPP1 (TAPP1-PH_{CT}) (Dowler *et al*., 2000; Thomas *et al*., 2001; Kimber *et al*., 2002). Using SPR, we compared the affinities of the p47*phox* PX domain and the TAPP1 PH_{CT} domain for POPC/POPE/PtdIns(3,4)P_2 vesicles. As previously reported (Dowler *et al*., 2000), the TAPP1-PH_{CT} has a high affinity for PtdIns(3,4)P_2, and this necessitated measurements with vesicles containing only 0.5% PtdIns(3,4)P_2. Under these conditions, the affinity of the TAPP1 PH_{CT} domain is 1.5 nM as compared with 2.6 μM for the p47*phox* PX domain (Table III). In addition to the difference in affinities, there is a difference in the modes of lipid interaction. The TAPP1-PH_{CT} affinity is dictated largely by the PtdIns(3,4)P_2 headgroup binding (Ferguson *et al*., 2000), whereas the p47*phox*-PX binds the soluble headgroup only very weakly (affinity >50 μM as measured by

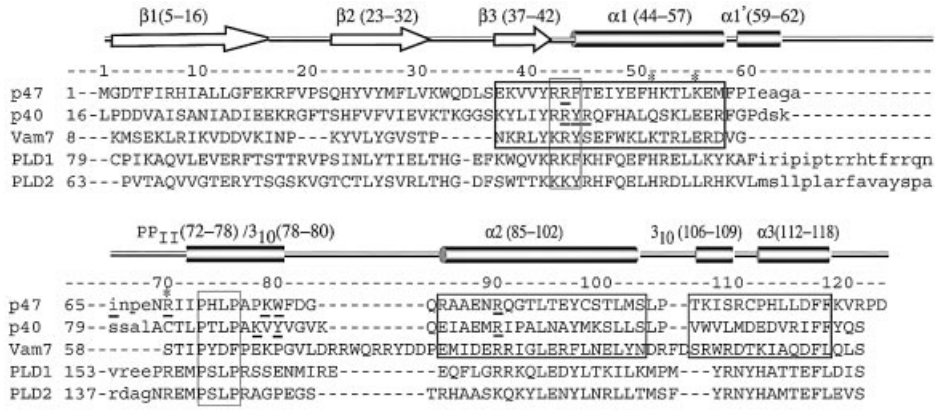

Fig. 5. Sequence alignment of several PX domains. The secondary structure elements and residue numbers of p47^{phox} are shown above its sequence. The p47^{phox} residues shown by mutagenesis to be involved in membrane binding and the p40^{phox} residues that interact with the bound PtdIns3P are underlined. The basic residues in the second anion-binding pocket of p47^{phox} are marked with asterisks. The regions containing the strongly conserved (R/K)-(R/K)-(Y/F) and PXXP motifs are boxed with thin lines. The portions of p40^{phox}, p47^{phox} and Vam7p that structurally superimpose the best are enclosed in boxes with thick lines. The sequences of PLD1 and PLD2 suggest that their PX domains, like p47^{phox}, may have a second anion-binding pocket.

Table II. Effect of phosphoinositides on membrane binding of p47^{phox}-PX determined by SPR analysis

Phosphoinositide	k_a (M^{-1} s^{-1})	k_d (s^{-1})	K_d (M)	Fold increase in K_d[a]
PtdIns(3,4)P_2	(1.6 ± 0.3) × 10^4	(6.1 ± 0.7) × 10^{-4}	(3.8 ± 0.8) × 10^{-8}	1
PtdIns(4,5)P_2	(9.0 ± 1.1) × 10^3	(8.5 ± 0.8) × 10^{-3}	(9.5 ± 3.4) × 10^{-7}	25
PtdIns(3,4,5)P_2	(8.8 ± 0.9) × 10^3	(7.3 ± 0.7) × 10^{-3}	(8.3 ± 1.2) × 10^{-7}	22
PtdIns3P	(7.8 ± 0.8) × 10^3	(7.1 ± 0.7) × 10^{-3}	(9.1 ± 1.3) × 10^{-7}	24
PtdIns4P	(7.8 ± 0.8) × 10^3	(8.1 ± 0.9) × 10^{-3}	(1.0 ± 1.5) × 10^{-6}	26
PtdIns5P	(9.8 ± 1.2) × 10^3	(6.9 ± 0.6) × 10^{-3}	(7.0 ± 1.1) × 10^{-7}	18

Values represent the mean and standard deviation from five determinations. All measurements were performed with POPC/POPE/phosphoinositide vesicles (77:20:3) in 20 mM Tris–HCl pH 7.4 containing 0.1 M KCl.
[a]Increase in K_d relative to binding to POPC/POPE/PtdIns(3,4)P_2 vesicles.

isothermal titration calorimetry, data not shown). These differences are likely to manifest themselves in the behaviours of the two domains in cells.

Distinct specificities of the two phospholipid-binding pockets in the p47^{phox} PX domain

The roles of the two phospholipid-binding pockets were clarified by measuring the binding of a series of site-specific mutants to vesicles containing PtdIns(3,4)P_2 and different anionic lipids. We first measured the binding of mutants to POPC/POPE/PtdIns(3,4)P_2 (77:20:3) vesicles by SPR analysis. Results are summarized in Table III. Clearly, mutations in the putative phosphoinositide-binding pocket strongly reduce binding to PtdIns(3,4)P_2-containing vesicles. Arg43, the putative 3-phosphate ligand, has the most decisive role in recognizing PtdIns(3,4)P_2. The R43Q mutation decreased the affinity for POPC/POPE/PtdIns(3,4)P_2 vesicles by 245-fold. The putative 4-phosphate ligand, Arg90, also has a substantial role in binding. The R90A mutation decreased the affinity for POPC/POPE/PtdIns(3,4)P_2 vesicles by 84-fold. The decreased membrane affinities of the R43Q and R90A mutants are due mostly to large increases in the k_d, consistent with our finding that specific phosphoinositide headgroup interactions primarily result in longer membrane residence time (Stahelin *et al*., 2002). The p47^{phox}-PX binding to PtdIns(3,4)P_2 and the importance of Arg90 was also apparent in semi-quantitative multilamellar vesicle (MLV) sedimentation assays (Figure 7). When compared with R43Q and R90A mutations, the mutation of a putative 1-phosphate ligand, K79A, showed a smaller impact on PtdIns(3,4)P_2 binding (a 6-fold reduction) (Table III). In contrast to mutations in the phosphoinositide-binding pocket, mutation of Arg70, which is the principal sulfate ligand in the second anion-binding pocket, resulted in only a 2-fold decrease in affinity for POPC/POPE/PtdIns(3,4)P_2 vesicles, indicating that PtdIns(3,4)P_2 does not interact productively with the second anion-binding pocket. Lastly, Lys52, which is remote from both sulfate-binding pockets, also has no influence on PtdIns(3,4)P_2 binding.

Given that the second sulfate-binding pocket is shallow, we thought that it might bind an anionic lipid with a smaller headgroup such as phosphatidic acid (PtdOH) or phosphatidylserine (PtdSer). To test this notion, we measured the binding of mutants to vesicles containing 1-palmitoyl-2-oleoyl-*sn*-glycero-3-phosphatidic acid (POPA) or 1-palmitoyl-2-oleoyl-*sn*-glycero-3-phosphoserine (POPS). Increasing POPA or POPS composition to 3 mol% in POPC/POPE/POPA(S) vesicles (i.e. 77:20:3) did not significantly enhance the affinity of p47^{phox}-PX (data not shown). However, 30 mol% of POPS in the vesicles was nearly as effective as 3 mol% PtdIns(3,4)P_2 in enhancing vesicle affinity of the p47^{phox}-PX (see Table III). Furthermore, 30 mol% POPA had an even more pronounced effect: the K_d for the p47^{phox}-PX for POPC/POPE/POPA (50:20:30) vesicles was 1.2 ± 0.3 nM. To assess the

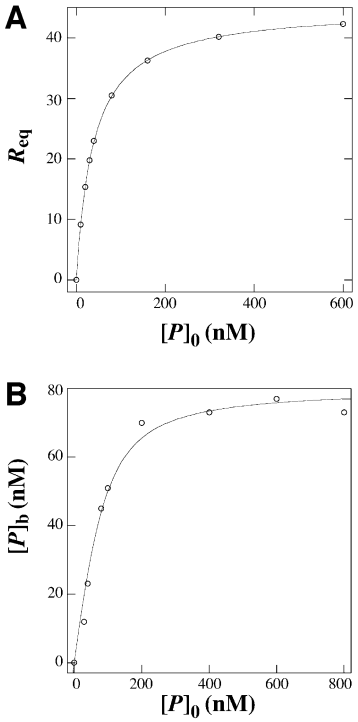

Fig. 6. Determination of the K_d for p47^{phox}-PX by equilibrium binding measurements. (**A**) Binding isotherms for p47^{phox}-PX and POPC/POPE/PtdIns(3,4)P_2 (77:20:3) vesicles from equilibrium SPR measurements. A solid line represents a theoretical curve constructed from R_{max} (45 ± 0.1) and K_d (38 ± 0.1 nM) values determined by non-linear least-squares analysis of the isotherm using an equation, $R_{eq} = R_{max}/(1 + K_d/P_0)$. (**B**) Binding isotherm for p47^{phox}-PX and beads coated with POPC/POPE/PtdIns(3,4)P_2 (77:20:3). Phospholipid-coated beads (1.5 μM bulk concentration) were incubated with ^{14}C-labelled p47^{phox}-PX (10–400 nM) in 20 mM Tris–HCl buffer pH 7.4 containing 0.1 M KCl and 1 μM BSA. A solid line represents a theoretical curve constructed from n (19 ± 1) and K_d (30 ± 7 nM) values determined by non-linear least-squares analysis of the isotherm using Equation 1.

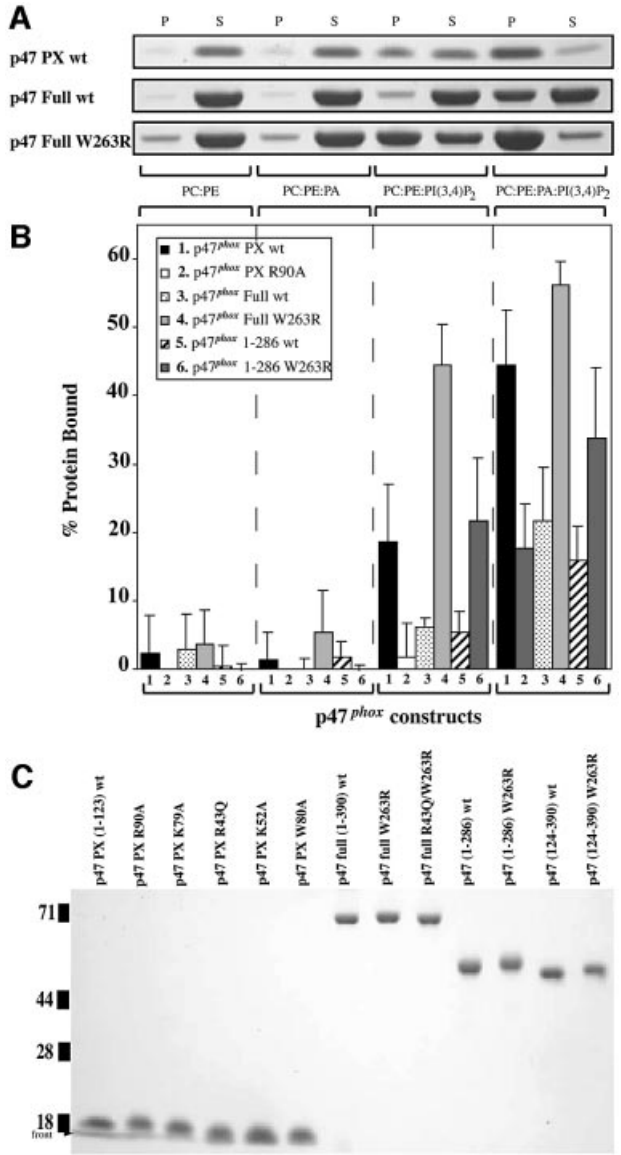

Fig. 7. Binding of p47^{phox} constructs to MLVs. (**A**) The proteins were incubated with MLVs containing 1 mM total lipid of POPC:POPE (50:50), POPC:POPE:POPA (47.5:47.5:5), POPC:POPE:PtdIns(3,4)P_2 (47.5:47.5:5) and POPE:POPE:POPA:PtdIns(3,4)P_2 (45:45:5:5). P and S indicate 'pellet' and 'supernatant' fractions after centrifugation. Samples were analysed by SDS–PAGE, and three representative gels for the p47^{phox}-PX, p47^{phox} full-length wild-type, and p47^{phox} full-length with the W263R mutation in the C-SH3 are shown. (**B**) The intensities of the stained 'pellet' bands were quantitated by densitometry, and the percentage of protein bound was determined. The values represent at least four independent measurements. (**C**) SDS–PAGE analysis of His_6-p47^{phox} constructs used in the binding studies. An estimated 0.5 μg of each protein was loaded on a 4–20% gradient SDS–polyacrylamide gel. The gel was stained with SimplyBlue SafeStain. All proteins were expressed with a His_6 affinity tag, and purified as described.

roles of the two binding pockets in PtdOH or PtdSer binding, we first measured the effects of critical mutants in each of the pockets on POPC/POPE/POPS (50:20:30) vesicles in the absence of phosphoinositide. As shown in Table III, a mutation in the phosphoinositide pocket (R90A) did not affect POPS-dependent binding. However, a mutation in the second anion-binding pocket (R70Q) decreased binding by 18-fold. This shows that only the second pocket binds POPS.

In order to determine whether both pockets can be occupied simultaneously by their preferred lipids, we carried out measurements using POPC/POPE/POPS/PtdIns(3,4)P_2 or POPC/POPE/POPA/PtdIns(3,4)P_2 (74:20:3:3) vesicles. When compared with POPC/POPE/PtdIns(3,4)P_2 (77:20:3) vesicles, the affinity of p47^{phox}-PX increased 63-fold when 3% POPA was included in the PtdIns(3,4)P_2-containing vesicles and 25-fold for 3% POPS (Table III). This indicates that simultaneous occupation of the two lipid-binding sites synergistically increases the membrane binding of p47^{phox}-PX [note that 3 mol% of POPA or POPS had little effect on the affinity of p47^{phox}-PX for POPC/POPE (80:20) vesicles]. The synergistic effect of PtdIns(3,4)P_2 and POPS increases the membrane affinity of the p47^{phox}-PX to about the same as the TAPP1-PH_{CT} affinity (Table III).

The p47^{phox}-PX mutants R43Q and R90A that showed 245- and 84-fold decreases, respectively, in affinity for POPC/POPE/PtdIns(3,4)P_2 (77:20:3) vesicles exhibited less pronounced 87- and 37-fold reductions, respectively, in affinity for POPC/POPE/POPS/PtdIns(3,4)P_2 (74:20:3:3) vesicles. A similar trend was seen with POPC/POPE/POPA/PtdIns(3,4)P_2 (74:20:3:3) vesicles. Thus, the occupation of the second anion site by POPA or POPS lessens

Table III. Binding parameters for p47^{phox}-PX and mutants determined from SPR analysis

Proteins	k_a (M^{-1} s^{-1})	k_d (s^{-1})	K_d (M)	Fold increase in K_d[a]
POPC/POPE/PtdIns(3,4)P_2 (77:20:3)				
p47^{phox}-PX	$(1.6 \pm 0.3) \times 10^4$	$(6.1 \pm 0.7) \times 10^{-4}$	$(3.8 \pm 0.8) \times 10^{-8}$	1
R43Q	$(7.0 \pm 0.6) \times 10^3$	$(6.5 \pm 0.7) \times 10^{-2}$	$(9.3 \pm 1.3) \times 10^{-6}$	245
K52A	$(1.5 \pm 0.2) \times 10^4$	$(6.0 \pm 0.8) \times 10^{-4}$	$(4.0 \pm 0.8) \times 10^{-8}$	1
I65A	$(1.3 \pm 0.2) \times 10^4$	$(2.8 \pm 0.4) \times 10^{-3}$	$(2.2 \pm 0.5) \times 10^{-7}$	6
R70Q	$(1.0 \pm 0.2) \times 10^4$	$(6.0 \pm 0.7) \times 10^{-4}$	$(6.0 \pm 1.4) \times 10^{-8}$	2
K79A	$(9.0 \pm 1.0) \times 10^3$	$(2.1 \pm 0.4) \times 10^{-3}$	$(2.3 \pm 0.5) \times 10^{-7}$	6
W80A	$(1.7 \pm 0.3) \times 10^5$	$(2.0 \pm 0.3) \times 10^{-3}$	$(1.1 \pm 0.3) \times 10^{-6}$	29
R90A	$(8.4 \pm 0.7) \times 10^3$	$(2.7 \pm 0.3) \times 10^{-2}$	$(3.2 \pm 0.4) \times 10^{-6}$	84
POPC/POPE/PtdIns(3,4)P_2 (79.5:20:0.5)				
TAPP1-PH_{CT}	$(1.6 \pm 0.4) \times 10^5$	$(2.4 \pm 0.5) \times 10^{-4}$	$(1.5 \pm 0.5) \times 10^{-9}$	1
p47^{phox}-PX	$(1.0 \pm 0.5) \times 10^4$	$(2.6 \pm 0.4) \times 10^{-2}$	$(2.6 \pm 1.4) \times 10^{-6}$	1700[b]
POPC/POPE/POPS/PtdIns(3,4)P_2 (49.5:20:30:0.5)				
p47^{phox}-PX	$(1.1 \pm 0.3) \times 10^5$	$(5.5 \pm 0.6) \times 10^{-4}$	$(5.0 \pm 1.5) \times 10^{-9}$	
POPC/POPE/POPS (50:20:30)				
p47^{phox}-PX	$(1.2 \pm 0.3) \times 10^5$	$(6.0 \pm 0.5) \times 10^{-3}$	$(5.0 \pm 1.3) \times 10^{-8}$	1
R70Q	$(2.3 \pm 0.4) \times 10^4$	$(2.1 \pm 0.2) \times 10^{-2}$	$(9.1 \pm 1.8) \times 10^{-7}$	18
R90A	$(1.1 \pm 0.2) \times 10^5$	$(7.0 \pm 0.8) \times 10^{-3}$	$(6.3 \pm 1.4) \times 10^{-8}$	1
POPC/POPE/POPS/PtdIns(3,4)P_2 (74:20:3:3)				
p47^{phox}-PX	$(9.6 \pm 0.9) \times 10^4$	$(1.4 \pm 0.2) \times 10^{-4}$	$(1.5 \pm 0.3) \times 10^{-9}$	1
R43Q	$(8.4 \pm 0.7) \times 10^4$	$(1.1 \pm 0.1) \times 10^{-2}$	$(1.3 \pm 0.2) \times 10^{-7}$	87
K52A	$(5.0 \pm 0.6) \times 10^4$	$(1.8 \pm 0.2) \times 10^{-4}$	$(3.6 \pm 0.6) \times 10^{-9}$	2
I65A	$(8.6 \pm 0.9) \times 10^4$	$(6.1 \pm 0.5) \times 10^{-4}$	$(7.1 \pm 0.9) \times 10^{-9}$	5
R70Q	$(8.5 \pm 0.8) \times 10^4$	$(3.1 \pm 0.5) \times 10^{-3}$	$(3.6 \pm 0.7) \times 10^{-8}$	24
K79A	$(8.0 \pm 0.7) \times 10^4$	$(3.8 \pm 0.4) \times 10^{-4}$	$(4.8 \pm 0.7) \times 10^{-9}$	3
R90A	$(7.1 \pm 0.8) \times 10^4$	$(3.9 \pm 0.3) \times 10^{-3}$	$(5.5 \pm 0.8) \times 10^{-8}$	37
POPC/POPE/POPA/PtdIns(3,4)P_2 (74:20:3:3)				
p47^{phox}-PX	$(1.5 \pm 0.3) \times 10^5$	$(9.0 \pm 0.8) \times 10^{-5}$	$(6.0 \pm 0.1) \times 10^{-10}$	1
R43Q	$(4.0 \pm 0.5) \times 10^4$	$(1.9 \pm 0.3) \times 10^{-3}$	$(4.8 \pm 1.0) \times 10^{-8}$	80
K52A	$(6.4 \pm 0.7) \times 10^4$	$(1.0 \pm 0.2) \times 10^{-4}$	$(1.7 \pm 0.4) \times 10^{-9}$	3
I65A	$(8.8 \pm 1.0) \times 10^4$	$(4.3 \pm 0.5) \times 10^{-4}$	$(4.1 \pm 0.7) \times 10^{-9}$	7
R70Q	$(3.8 \pm 0.3) \times 10^4$	$(5.0 \pm 0.4) \times 10^{-4}$	$(1.3 \pm 0.1) \times 10^{-8}$	22
K79A	$(9.0 \pm 0.8) \times 10^4$	$(2.4 \pm 0.4) \times 10^{-4}$	$(2.6 \pm 0.5) \times 10^{-9}$	4
W80A	$(6.6 \pm 0.7) \times 10^4$	$(2.0 \pm 0.4) \times 10^{-3}$	$(3.0 \pm 0.7) \times 10^{-8}$	50
R90A	$(5.8 \pm 0.6) \times 10^4$	$(1.4 \pm 0.3) \times 10^{-3}$	$(1.6 \pm 0.4) \times 10^{-8}$	27

Values represent the mean and standard deviation from five determinations. All measurements were performed in 20 mM Tris–HCl pH 7.4 containing 0.1 M KCl.
[a]Increase in K_d relative to the wild-type binding to the same vesicles.
[b]Increase in K_d relative to the TAPP1-PH_{CT} binding to the same vesicles.

the deleterious effect of mutations in the phosphoinositide-binding site, underscoring the complementary nature of the two binding sites. In contrast, R70Q, which has 50% of wild-type affinity for POPC/POPE/PtdIns(3,4)P_2 (77:20:3) vesicles, has >20-fold reduced affinity for POPC/POPE/POPS (or POPA)/PtdIns(3,4)P_2 (74:20:3:3) vesicles. Together, these data indicate that POPA or POPS show a strong preference for the second anion-binding site and that PtdIns(3,4)P_2 does not interact effectively with this anion-binding site.

Hydrophobic residues surrounding the lipid-binding pockets contribute to membrane affinity

Both the PtdIns(3,4)P_2 and the secondary anion-binding pockets are flanked by exposed hydrophobic residues that protrude from the putative membrane-binding surface. Mutation of Trp80, which is in the membrane insertion loop between the two lipid-binding pockets, reduces the affinity 29- or 50-fold depending on the vesicle composition (Table III). Mutation of Ile65 (I65A), which is adjacent to the anionic-lipid-binding pocket, reduced the affinity 5- to 7-fold (Table III). This suggests that these hydrophobic residues have a role in membrane penetration during binding.

The PX domain lipid binding is masked in the full-length p47^{phox}

It was reported previously that the C-SH3 of p47^{phox} interacts with the PXXP motif of the PX domain (Hiroaki *et al*., 2001). In order to determine the effect of this interaction on membrane binding, we compared binding of the full-length p47^{phox} with binding by the isolated PX domain. Remarkably, the full-length protein shows no significant interaction with PtdIns(3,4)P_2 in MLV sedimentation assays (Figure 7). SPR measurements show that the affinity of the full-length p47^{phox} for POPC/POPE/PtdIns(3,4)P_2 (77:20:3) vesicles is 34-fold lower than that of the isolated PX domain (Table IV). However, the W263R mutation in the C-SH3 that was reported to abrogate binding to p47^{phox}-PX resulted in a huge increase in binding (540-fold) compared with the full-length wild-type protein, suggesting that the mutation unmasks the lipid-binding surface of the PX domain. Lipid binding by

Table IV. Binding parameters for p47^{phox} and p47^{phox}-PX determined from SPR analysis

Proteins	k_a (M^{-1} s^{-1})	k_d (s^{-1})	K_d (M)	Fold increase in K_d[a]
POPC/POPE/PtdIns(3,4)P_2 (77:20:3)				
p47^{phox}-PX	(1.6 ± 0.3) ×10^4	(6.1 ± 0.7) × 10^{-4}	(3.8 ± 0.8) × 10^{-8}	1
p47^{phox}	(8.7 ± 0.7) × 10^3	(1.1 ± 0.2) × 10^{-2}	(1.3 ± 0.3) × 10^{-6}	34
W263R p47^{phox}	(4.2 ± 0.4) × 10^4	(1.0 ± 0.1) × 10^{-4}	(2.4 ± 0.3) × 10^{-9}	0.06
R43Q/W263R p47^{phox}	(1.6 ± 0.2) × 10^4	(1.8 ± 0.2) × 10^{-2}	(1.1 ± 0.2) × 10^{-6}	29
5SE p47^{phox} [S(303,304,328,359,370)E]	(3.8 ± 0.7) × 10^4	(5.0 ± 0.4) × 10^{-4}	(1.3 ± 0.3) × 10^{-8}	0.34
R43Q/5SE p47^{phox}	(1.3 ± 0.4) × 10^4	(1.3 ± 0.2) × 10^{-2}	(1.0 ± 0.3) × 10^{-6}	26

Values represent the mean and standard deviation from five determinations. All measurements were performed in 20 mM Tris–HCl pH 7.4 containing 0.1 M KCl.
[a]Increase in K_d relative to the binding of the p47^{phox} PX domain to the same vesicles.

p47^{phox}-1–286, a construct containing the PX domain and the two SH3 domains but lacking the C-terminal tail, is also unmasked only in the W263R variant (as judged by MLV binding, Figure 7), but the binding was somewhat weaker than that of the full-length W263R. A mutation in the PtdIns(3,4)P_2-binding pocket (R43Q) of the unmasked full-length protein (R43Q/W263R) reduced binding to approximately the same level as the masked, wild-type form (Table IV). Consistent with this, a construct lacking the PX domain either with or without the W263R mutation shows no measurable binding in the MLV assay (data not shown). These results indicate that high affinity lipid binding of the full-length p47^{phox} depends on the PX domain interacting with phospholipids, although other regions of the protein also contribute. The observation that the 1–286 W263R p47^{phox} has a somewhat weaker membrane binding than the full-length W263R p47^{phox} suggests that the C-terminal tail (287–390) accounts for some of these additional interactions.

A mimic of the phosphorylated state of p47 is 'open' and capable of binding PtdIns(3,4)P_2

The p47^{phox} subunit is phosphorylated on up to nine sites in the C-terminal tail. Functionally important sites of phosphorylation include serines 303, 304, 328, 359 and 370. Mimicking phosphorylation by replacing serines 303, 304 and 328 with glutamates led to an open conformation of p47^{phox} that was able to bind to p22^{phox} (Ago *et al.*, 1999). Replacement of serines 359 and 370 with alanines results in a p47^{phox} that has dramatically reduced phosphorylation and fails to translocate to membranes, but mutation of these residues into glutamates results in a p47^{phox} subunit for which normal phosphorylation and translocation are observed (Johnson *et al.*, 1998). To examine the effect of phosphorylation on phosphoinositide binding, we made a quintuple mutant S303E/S304E/S228E/S359E/S370E (p47^{phox}-5SE), which mimics the phosphorylated form. The p47^{phox}-5SE mutant binds PtdIns(3,4)P_2 with an affinity that is ~100-fold greater than that of the wild-type p47^{phox} and only ~5-fold weaker than that of the W263R mutant (Table IV). Like the W263R mutant of the C-SH3, this phosphorylation mimic appears to have an 'open' conformation with an unmasked PX domain, in contrast to the full-length wild-type p47^{phox}, even though none of the sites of pseudo-phosphorylation are within the C-SH3.

Discussion

Synergistic membrane binding of the PX domain using two distinct lipid-binding pockets

The structure of the p47^{phox} PX domain and the lipid-binding studies of the wild-type and site-specific mutants reveal that the domain has two distinct lipid-binding sites. Simultaneous occupancy of the phosphoinositide site by PtdIns(3,4)P_2 and the second anion-binding site by PtdOH (or less preferentially PtdSer) leads to a great synergistic increase in membrane affinity. The ability of PtdOH to increase p47^{phox} membrane binding substantially is consistent with reports that PtdOH can interact directly with cytosolic subunits of NADPH oxidase and activate it via a kinase-independent mechanism (Erickson *et al.*, 1999; Palicz *et al.*, 2001). One interesting question is whether PX domains of p40^{phox} and p47^{phox} can synergize in membrane binding in the context of the p40^{phox}–p47^{phox}–p67^{phox} heterotrimer and, if so, are the specific ligands of the two domains [PtdIns(3,4)P_2, PtdIns3P and PtdOH] present at the same time and place.

Masking of the lipid-binding surface of the p47^{phox} PX domain by intramolecular interactions

The p47^{phox} subunit contains an N-terminal PX domain followed by two SH3 domains (N-SH3 and C-SH3) and a C-terminal tail. The N-SH3 interacts with a proline-rich region in the C-terminus of p22^{phox} and is necessary for both translocation of the cytosolic complex to the membrane and activation of the NADPH oxidase (Leto *et al.*, 1994; Sumimoto *et al.*, 1994, 1996; Leusen *et al.*, 1996; Huang and Kleinberg, 1999). However, in the context of full-length, unphosphorylated p47^{phox}, the N-SH3 is masked by interaction with the p47^{phox} C-terminal tail. The phosphorylation of p47^{phox} causes a conformational change (Swain *et al.*, 1997) that releases the C-terminal tail from its association with the tandem SH3 domains, freeing the N-SH3 to bind the flavocytochrome (Ago *et al.*, 1999; Huang and Kleinberg, 1999). It has been shown that the C-SH3 can interact with the p47^{phox} PX domain via the PXXP motif (Hiroaki *et al.*, 2001). However, because the C-SH3 does not interact with the flavocytochrome b_{558}, it was not clear what might be the consequence of this interaction for the function of the oxidase. A study using a cell-free assay suggested that the role of the PX domain is not simply to mask the C-SH3 because a p47^{phox} construct

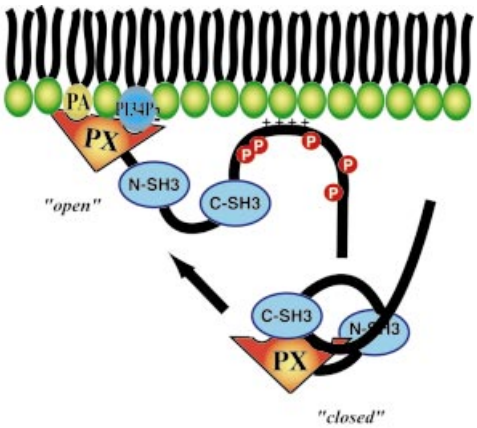

Fig. 8. Activation-dependent membrane binding of p47^{phox}. In the resting state, p47^{phox} is locked in a closed state by an intramolecular interaction between the C-SH3 and the PXXP motif of the PX domain, preventing phospholipid binding. Phosphorylation of sites in the C-terminal tail releases the lock, freeing the PX domain to bind to membranes with both PX phospholipid-binding pockets and a basic region in the C-terminal tail.

lacking the PX domain was not able to activate the oxidase (Hata *et al*., 1998).

We demonstrate here that the full-length p47^{phox} in its basal, 'closed' form does not bind phosphoinositides due to a masking of the PX domain by the C-SH3. A site-specific mutation (W263R) in the C-SH3 of p47^{phox} unmasks the lipid-binding surface of the PX domain. However, this mutant has an even higher membrane affinity than the isolated PX, suggesting that additional sites of membrane interaction, probably in the C-terminal tail, are exposed in the full-length protein.

Phosphorylation of p47^{phox} leads to an open conformation with an unmasked PX domain

Formation of the active oxidase complex is critically dependent on phosphorylation of p47^{phox} (Heyworth *et al*., 1989; Rotrosen and Leto, 1990; El Benna *et al*., 1994; Johnson *et al*., 1998). Our binding study of a quintuple phosphorylation mimic suggests that the phosphorylation-induced 'open' conformation of p47^{phox} that enables interaction of the N-SH3 with p22^{phox} also enables interaction of the p47^{phox} PX domain with PtdIns(3,4)P_2, as illustrated schematically in Figure 8. This would be consistent with observations that phosphorylation of p47^{phox} results in its translocation to the plasma membrane *in vivo* (Leto *et al*., 1994; Sumimoto *et al*., 1994, 1996; Leusen *et al*., 1996; Huang and Kleinberg, 1999).

Conclusions

The functional role of the two phospholipid-binding sites of the p47^{phox} PX domain *in vivo* needs to be determined. The non-overlapping specificities of the phospholipid-binding pockets may affect the types of membranes to which p47^{phox} binds or the timing and duration of NADPH oxidase activation in relation to levels of PtdIns(3,4)P_2 or PtdOH. A previous report had shown that the p47^{phox}-PX could be visualized in membrane ruffles that form in response to insulin-like growth factor 1 (Zhan *et al*., 2002). However, the study provided no quantification to indicate that the domain was enriched in these structures. Although it is uncertain whether it is the driving force in translocation to plasma membranes, the p47^{phox}-PX may be important for the regulatory complex achieving a productive orientation on the membrane to enable activation of the oxidase. The results presented here establishing the structure, binding characteristics and phosphorylation-dependent regulation of two distinct phospholipid-binding sites in the p47^{phox} PX domain provide a foundation upon which further studies aimed at correlating membrane binding and NADPH oxidase activity *in vivo* can build.

Materials and methods

Materials

POPC, POPS, POPE, egg L-α phosphatidic acid, brain L-α phosphatidylcholine and brain L-α phosphatidylethanolamine were from Avanti Polar Lipids (Alabaster, AL). 1,2-dipalmitoyl derivatives of PtdIns3P, phosphatidylinositol 4-phosphate (PtdIns4P), phosphatidylinositol-5-phosphate (PtdIns5P), PtdIns(3,4)P_2, phosphatidylinositol 4,5-bisphosphate [PtdIns(4,5)P_2], and phosphatidylinositol 3,4,5-trisphosphate [PtdIns(3,4,5)P_3] used in SPR measurements were a generous gift of Dr Karol Bruzik of the University of Illinois at Chicago. For MLV sedimentation assays, di-C_{16}PtdIns(3,4)P_2 and di-C_{16}PtdIns3P were purchased from Echelon Research Labs (P-3416 and P-3016). For SPR studies, phospholipid concentrations were determined by phosphate analysis (Kates, 1986). For MLV sedimentation assays, lipid concentrations were based on the masses supplied by the manufacturer. The Liposofast microextruder and 100 nm polycarbonate filters were from Avestin (Ottawa, Ontario, Canada). Fatty acid-free bovine serum albumin (BSA) was from Bayer, Inc. (Kankakee, IL). [3-(3-cholamidopropyl)-dimethylammonio]-1-propane-sulfonate and octyl glucoside were from Sigma and Fisher Scientific, respectively. Pioneer L1 sensor chip was from Biacore AB (Piscataway, NJ).

Protein expression and purification

A PCR product encoding residues 1–123 of human p47^{phox} was cloned into vector pJL using *Nde*I–*Hin*dIII sites. The vector codes for an MAH_6 affinity tag immediately preceding residue Met1. Protein was expressed in *Escherichia coli* strain C41(DE3), grown in 2× TY/Amp at 37°C to a density of 1 OD_{600}, then induced with 1 mM isopropyl-β-D-thiogalactopyranoside (IPTG) at 22°C for 5 h. The protein for crystallography was purified by Ni^{2+} affinity, heparin–Sepharose and gel filtration chromatography. For mutants used in binding studies, the heparin chromatography was omitted. The gel filtration was run in a buffer consisting of 20 mM Tris pH 7.4 (4°C), 100 mM NaCl. The protein was concentrated to 4.5 mg/ml and frozen in liquid nitrogen. Selenomethionine-substituted (Se-Met) protein was grown in the methionine-requiring auxotrophic strain 834(DE3) using a medium consisting of 2× M9 minimal medium supplemented with 1 mg/l riboflavin, 1 mg/l niacinamide, 1 mg/l thiamine, 0.1 mg/l pyridoxine monohydrate, 0.4% D(+)-glucose, 2 mM $MgSO_4$, 25 mg/l $FeSO_4$, 40 mg/l of each amino acid except methionine, 80 mg/l seleno-D,L-methionine and 0.1 g/l ampicillin. Mutations in the p47^{phox}-PX were constructed using the overlap extension method. All of the mutants except I65A were cloned in the pJL vector. The I65A mutant was subcloned into the pET21a vector containing a His_6 tag. The full-length p47^{phox}, the 1–286 deletion variant, the 124–390 deletion variant and mutations of these constructs were cloned with the same N-terminal tag as the p47^{phox}-PX (MAH_6). The TAPP1-PH_{CT} was cleaved from a GST fusion and purified as previously described (Thomas *et al*., 2001). All constructs were checked by DNA sequencing. Protein concentration was determined by OD_{280} using calculated molar extinction coefficients (for crystallography and MLV sedimentation assays) or using the Pierce BCA method (for SPR studies).

Protein refolding

The R70Q mutant in the p47^{phox}-PX was expressed as an inclusion body and thus needed to be refolded. The inclusion body pellet was resuspended in 25 ml Tris–HCl pH 8.0 containing 50 mM NaCl, 0.8% (v/v) Triton X-100 and 0.8% (w/v) sodium deoxycholate. After centrifugation at 48 000 *g* for 15 min, the pellet was resuspended in 25 ml of 50 mM Tris–HCl pH 8.0 containing 5 M urea. The pellet was stirred at room temperature for 1 h, and then the suspension was

centrifuged at 100 000 *g* for 25 min. The supernatant was collected and dialysed against 50 mM Tris–HCl pH 8.0 and 1.5 M urea for 16 h, and then against 50 mM Tris–HCl pH 8.0 for 24 h. The refolded R70Q mutation was purified by Ni^{2+} affinity and gel filtration chromatography.

Crystallization

The protein was crystallized in sitting drops using the vapour diffusion method. The drops contained 1 µl of protein mixed with 1 µl of reservoir solution. Initial crystals were obtained from Hampton Crystal Screen II, condition 42. The optimized reservoir solution consisted of 1.0 M NH_2SO_4, 0.1 M Tris pH 8.5 (4°C) and 12% glycerol. Crystals used for data collection were grown by hair seeding. The Se-Met protein crystallized in space group *I*222 with cell dimensions a = 74.2 Å, b = 92.2 Å, c = 144.0 Å.

Diffraction data collection

For data collection, crystals were cryo-protected in paratone-N (Hampton). Data for the Se-Met-substituted crystals were collected at wavelengths corresponding to the peak and inflection point of the fluorescence spectrum for Se (12.664 and 12.662 keV, respectively). Data were processed with MOSFLM (Leslie, 1992) and CCP4 (1994). Se sites were located and refined using autoSHARP (C.Vonrhein, E.Blanc, P.Roversi and G.Bricogne, in preparation) and SHARP (de La Fortelle and Bricogne, 1997). Solvent flattening was carried out with a solvent content of 44.6%. The asymmetric unit of the crystal consists of three molecules related to each other by a 3-fold rotation axis. The overall fold of the p47^{phox}-PX from the crystal structure agrees with the fold that was determined by NMR (Hiroaki *et al*., 2001); however, the NMR structure was not sufficiently similar to be useful as a model for molecular replacement. The models were built independently for the three chains in the asymmetric unit then refined using REFMAC (Murshudov *et al*., 1997) with isotropic *B*-factors and wARP (Perrakis *et al*., 1999). All residues in chain A of the trimer are visible in the electron density, while the three N-terminal residues are disordered in chains B and C. The N-terminal MAH_6 tag was disordered for all three chains. The loop between β1 and β2 (residues 16–22) is disordered in chain C. Non-crystallographic symmetry (NCS) was tightly restrained for residues not involved in crystal contacts during the initial stages of refinement. In the later stages of refinement, the NCS restraints were relaxed and finally removed. At each stage of relaxing the NCS restraints, the free *R*-factor decreased. Table I gives statistics for data collection and refinement.

MLV sedimentation binding assay

Protonation of di-C_{16}PtdIns(3,4)P_2 was essential for obtaining reproducible lipid binding. Prior to use in the assay, solid di-C_{16}PtdIns(3,4)P_2 was resuspended in $CHCl_3$:MeOH:1 M HCl (volume ratios 2:1:0.01), dried with argon, then vacuum desiccated for 1 h, followed by three cycles of chloroform resuspension and desiccation and finally storage in chloroform at –70°C. Phospholipids in chloroform were mixed, dried and desiccated under vacuum for 1 h. The phospholipids were then resuspended in 500 µl of binding buffer [20 mM Tris pH 7.4, 100 mM NaCl, 1 mM dithiothreitol (DTT)] and rehydrated on ice for 2 h. The lipid mixture was then vortexed to produce MLVs. Protein stock and MLVs were mixed in 100 µl reactions to yield solutions containing 1 mM total lipid and 5 µM protein. The reactions were incubated for 15 min (20°C), then centrifuged for 10 min at 14 000 r.p.m. in a microfuge at room temperature. Supernatants were removed carefully and the pellets were resuspended in SDS sample buffer. Both the pellets and the supernatants were analysed by SDS–PAGE. Gels were stained in SimplyBlue SafeStain (Invitrogen), and quantitated with a ChemiGenius densitometer (SynGene) using GeneTools analysis software.

SPR experiments

A detailed protocol for coating the L1 sensor chip has been described elsewhere (Bittova *et al*., 2001; Stahelin and Cho, 2001). Briefly, after washing the sensor chip surface, 90 µl of 0.5 mM vesicles of a given composition [e.g. POPC/POPE/PtdIns(3,4)P_2 = 77:20:3)] were injected at 5 µl/min to give a response of 4000 RU. Similarly, a control surface was coated with the same vesicles minus the phosphoinositide of interest (e.g. POPC/POPE = 80:20) to give the same RU response as the active binding surface. This control surface was selected over the bare chip surface to circumvent any potential artefacts caused by the hydrophobic nature of the L1 chip. No binding was detected to this surface beyond the refractive index change for p47^{phox}-PX and other proteins used. Each lipid layer was stabilized by injecting 10 µl of 50 mM NaOH three times at 100 µl/min, which showed no decrease in lipid signal after the second injection. The coating efficiency of each surface was tested using a 25 µl injection of 0.1 mg/ml BSA. The BSA response was ~100 RU compared with 1200 RU of BSA for an uncoated chip surface. Control experiments with vesicles containing 5-carboxyfluorescein confirmed that vesicles remained intact on the chip. After stabilization of signal (i.e. <0.3 RU/min drift), experiments were peformed at 60 µl/min. A 90 µl aliquot of protein in 20 mM Tris pH 7.4 containing 0.1 M KCl was injected to give an association time of 90 s, while the dissociation was monitored for 500 s. The protein concentrations used were within a 10-fold range above and below the K_d values listed in Tables II–IV. After sensorgrams were obtained for five or more concentrations of each protein and corrected for refractive index changes, the association and dissociation phases of all sensorgrams were globally fit to a 1:1 Langmuir binding model: protein + (protein-binding site on vesicle) ↔ (complex), using BIAevaluation 3.0 software (Biacore). The association phase was analysed using the equation:

$$R = [k_aC/(k_aC + k_d)]\ R_{max}\ (1 - e^{-(k_aC + k_d)(t - t_0)}) + RI$$

where RI = refractive index change, R_{max} is the theoretical binding capacity, C is analyte concentration, k_a is the association rate constant, and t_0 is the time at start of fit data. The dissociation phase was analysed using an equation:

$$R = R_0 e^{-k_d(t - t_0)}$$

where k_d is the dissociation rate constant and R_0 is the response at the start of fit data. The dissociation constant (K_d) was then calculated from the equation, $K_d = k_d/k_a$. It should be noted that in our SPR analysis, K_d is defined in terms of not the molarity of phospholipids but the molarity of protein-binding sites on the vesicle. Thus, if each protein-binding site on the vesicle is composed of n lipids, nK_d is the dissociation constant in terms of molarity of lipid monomer (Cho *et al*., 2001). Due to difficulty involved in accurate determination of the concentration of lipids coated on the sensor chip, however, only K_d was determined in our SPR analysis and the relative affinity was calculated as a ratio of K_d values assuming that n values are essentially the same for wild-type and mutants. The 1:1 Langmuir binding model gives a good fit to the data with random residuals. Each measurement was repeated three or more times to calculate a standard deviation.

To verify the K_d determined from kinetic measurements for p47^{phox}-PX binding to POPC/POPE/PtdIns(3,4)P_2 (77:20:3) vesicles, we also performed equilibrium SPR measurements. For this purpose, the flow rate was reduced to 1 µl/min, and 90 µl of p47^{phox}-PX (10–600 nM) was injected and bound to a saturating value. These saturating (equilibrium) values (R_{eq}) were then plotted versus protein concentration ($[P]_0$) and the K_d value was determined by a non-linear least-squares analysis of the binding isotherm using the equation:

$$R_{eq} = R_{max}/(1 + K_d/([P]_0))$$

where R_{max} is a maximal R_{eq} value. Furthermore, n and K_d values were determined for the binding of radiolabelled p47^{phox}-PX to hydrophobic beads coated with POPC/POPE/PtdIns(3,4)P_2 (77:20:3) as described previously (Cho *et al*., 2001). Radiolabelling of the p47^{phox}-PX was performed as described (Stahelin *et al*., 2002). Parameters n and K_d were determined by non-linear least-squares analysis of the bound ($[P]_b$) versus $[P]_0$ plot using a standard binding equation, Equation 1 (Cho *et al*., 2001):

$$[P]_b = \frac{[P]_o + K_d + [PL]_o/n - \sqrt{([P]_o + K_d + [PL]_o/n)^2 - 4[P]_o[PL]_o/n}}{2} \quad (1)$$

where $[PL]_o$ represents total phospholipid concentration. The K_d value for p47^{phox}-PX determined from non-linear least square analysis of the binding isotherms (30 ± 7 nM) is comparable with that determined from the kinetic SPR analysis under the same condition (38 nM). The n value (19 ± 1) for p47^{phox}-PX suggests that each molecule interacts with ~19 phospholipid molecules. Thus the apparent dissociation constant in terms of total lipid concentration (nK_d) is ~0.6 µM for the p47^{phox}-PX.

Acknowledgements

We would like to thank Karol S.Bruzik for generous gift of phosphoinositides for SPR studies, Aura Burian for preparing the I65A mutant, Dario Alessi for providing a TAPP1 plasmid, Gordon Leonard

and Raimond Ravelli for their assistance with data collection at ESRF beamlines ID29 and ID14-4, and Phil Hawkins, Len Stephens and Chris Ellson for valuable discussions. The work was supported by a grant from the British Heart Foundation (to R.L.W.) and a National Institutes of Health grant GM53987 (to W.C.).

References

Ago,T., Nunoi,H., Ito,T. and Sumimoto,H. (1999) Mechanism for phosphorylation-induced activation of the phagocyte NADPH oxidase protein p47^{phox}. *J. Biol. Chem.*, **274**, 33644–33653.

Ago,T., Takeya,R., Hiroaki,H., Kuribayashi,F., Ito,T., Kohda,D. and Sumimoto,H. (2001) The PX domain as a novel phosphoinositide-binding module. *Biochem. Biophys. Res. Commun.*, **287**, 733–738.

Babior,B.M. (1999) NADPH oxidase: an update. *Blood*, **93**, 1464–1476.

Bittova,L., Stahelin,R.V. and Cho,W. (2001) Roles of ionic residues of the C1 domain in protein kinase C-α activation and the origin of phosphatidylserine specificity. *J. Biol. Chem.*, **276**, 4218–4226.

Bravo,J. *et al*. (2001) The crystal structure of the PX domain from p40^{phox} bound to phosphatidylinositol 3-phosphate. *Mol. Cell*, **8**, 829–839.

CCP4 (1994) Collaborative Computing Project Number 4: a suite of programs for protein crystallography. *Acta Crystallogr. D*, **50**, 760–763.

Cho,W., Bittova,L. and Stahelin,R.V. (2001) Membrane binding assays for peripheral proteins. *Anal. Biochem.*, **296**, 153–161.

de La Fortelle,E. and Bricogne,G. (1997) Maximum-likelihood heavy-atom parameter refinement for multiple isomorphous replacement and multiwavelength anomalous diffraction methods. *Methods Enzymol.*, **276**, 472–494.

Dowler,S., Currie,R.A., Campbell,D.G., Deak,M., Kular,G., Downes, C.P. and Alessi,D.R. (2000) Identification of pleckstrin-homology-domain-containing proteins with novel phosphoinositide-binding specificities. *Biochem. J.*, **351**, 19–31.

Dusi,S., Donini,M. and Rossi,F. (1996) Mechanisms of NADPH oxidase activation: translocation of p40^{phox}, Rac1 and Rac2 from the cytosol to the membranes in human neutrophils lacking p47^{phox} or p67^{phox}. *Biochem. J.*, **314**, 409–412.

El Benna,J., Faust,L.P. and Babior,B.M. (1994) The phosphorylation of the respiratory burst oxidase component p47^{phox} during neutrophil activation. *J. Biol. Chem.*, **269**, 23431–23436.

Ellson,C.D. *et al*. (2001) PtdIns(3)P regulates the neutrophil oxidase complex by binding to the PX domain of p40^{phox}. *Nat. Cell Biol.*, **3**, 679–682.

Erickson,R.W., Langel-Peveri,P., Traynor-Kaplan,A.E., Heyworth,P.G. and Curnutte,J.T. (1999) Activation of human neutrophil NADPH oxidase by phosphatidic acid or diacylglycerol in a cell-free system. Activity of diacylglycerol is dependent on its conversion to phosphatidic acid. *J. Biol. Chem.*, **274**, 22243–22250.

Ferguson,K.M., Kavran,J.M., Sankaran,V.G., Fournier,E., Isakoff,S.J., Skolnik,E.Y. and Lemmon,M.A. (2000) Structural basis for discrimination of 3-phosphoinositides by pleckstrin homology domains. *Mol. Cell*, **6**, 373–384.

Hata,K., Ito,T., Takeshige,K. and Sumimoto,H. (1998) Anionic amphiphile-independent activation of the phagocyte NADPH oxidase in a cell-free system by p47^{phox} and p67^{phox}, both in C terminally truncated forms. *J. Biol. Chem.*, **273**, 4232–4236.

Heyworth,P.G. and Cross,A.R. (2002) Chronic granulomatous disease mutations and the PX domain. *Nat. Cell Biol.*, **4**, E110.

Heyworth,P.G., Shrimpton,C.F. and Segal,A.W. (1989) Localization of the 47 kDa phosphoprotein involved in the respiratory-burst NADPH oxidase of phagocytic cells. *Biochem. J.*, **260**, 243–248.

Heyworth,P.G., Curnutte,J.T., Nauseef,W.M., Volpp,B.D., Pearson, D.W., Rosen,H. and Clark,R.A. (1991) Neutrophil nicotinamide adenine dinucleotide phosphate oxidase assembly. Translocation of p47-phox and p67-phox requires interaction between p47-phox and cytochrome b558. *J. Clin. Invest.*, **87**, 352–356.

Hiroaki,H., Ago,T., Ito,T., Sumimoto,H. and Kohda,D. (2001) Solution structure of the PX domain, a target of the SH3 domain. *Nat. Struct. Biol.*, **8**, 526–530.

Huang,J. and Kleinberg,M.E. (1999) Activation of the phagocyte NADPH oxidase protein p47(phox). Phosphorylation controls SH3 domain-dependent binding to p22(phox). *J. Biol. Chem.*, **274**, 19731–19737.

Johnson,J.L., Park,J.W., El Benna,J., Faust,L.P., Inanami,O. and Babior,B.M. (1998) Activation of p47(PHOX), a cytosolic subunit of the leukocyte NADPH oxidase—phosphorylation of Ser-359 or Ser-370 precedes phosphorylation at other sites and is required for activity. *J. Biol. Chem.*, **273**, 35147–35152.

Kanai,F., Liu,H., Field,S.J., Akbary,H., Matsuo,T., Brown,G.E., Cantley,L.C. and Yaffe,M.B. (2001) The PX domains of p47phox and p40phox bind to lipid products of PI(3)K. *Nat. Cell Biol.*, **3**, 675–678.

Kates,M. (1986) *Techniques of Lipidology*. Elsevier, Amsterdam, pp. 114–115.

Kim,Y., Lichtenbergova,L., Snitko,Y. and Cho,W. (1997) A phospholipase A2 kinetic and binding assay using phospholipid-coated hydrophobic beads. *Anal. Biochem.*, **250**, 109–116.

Kimber,W.A. *et al*. (2002) Evidence that the tandem-pleckstrin-homology-domain-containing protein TAPP1 interacts with Ptd(3,4)P2 and the multi-PDZ-domain-containing protein MUPP1 *in vivo*. *Biochem. J.*, **361**, 525–536.

Lapouge,K., Smith,S.J., Groemping,Y. and Rittinger,K. (2002) Architecture of the p40–p47–p67^{phox} complex in the resting state of the NADPH oxidase: a central role for p67^{phox}. *J. Biol. Chem.*, **277**, 10121–10128.

Leslie,A.G.W. (1992) Recent changes to the MOSFLM package for processing film and image plate data. *Joint CCP4 and ESF-EACMB Newsletter on Protein Crystallography*, Daresbury Laboratory, Warrington, UK, Vol. 26.

Leto,T.L., Adams,A.G. and de Mendez,I. (1994) Assembly of the phagocyte NADPH oxidase: binding of Src homology 3 domains to proline-rich targets. *Proc. Natl Acad. Sci. USA*, **91**, 10650–10654.

Leusen,J.H.W., Verhoeven,A.J. and Roos,D. (1996) Interactions between the components of the human NADPH oxidase: a review about the intrigues in the phox family. *Frontiers Biosci.*, **1**, d72–d90.

Lu,J., Garcia,J., Dulubova,I., Sudhof,T.C. and Rizo,J. (2002) Solution structure of the Vam7p PX domain. *Biochemistry*, **41**, 5956–5962.

Mayer,B.J. (2001) SH3 domains: complexity in moderation. *J. Cell Sci.*, **114**, 1253–1263.

McAdara Berkowitz,J.K., Catz,S.D., Johnson,J.L., Ruedi,J.M., Thon,V. and Babior,B.M. (2001) JFC1, a novel tandem C2 domain-containing protein associated with the leukocyte NADPH oxidase. *J. Biol. Chem.*, **276**, 18855–18862.

Murshudov,G.N., Vagin,A.A. and Dodson,E.J. (1997) Refinement of macromolecular structures by the maximum-likelihood method. *Acta Crystallogr. D*, **53**, 240–255.

Palicz,A., Foubert,T.R., Jesaitis,A.J., Marodi,L. and McPhail,L.C. (2001) Phosphatidic acid and diacylglycerol directly activate NADPH oxidase by interacting with enzyme components. *J. Biol. Chem.*, **276**, 3090–3097.

Perrakis,A., Morris,R. and Lamzin,V.S. (1999) Automated protein model building combined with iterative structure refinement. *Nat. Struct. Biol.*, **6**, 458–463.

Reeves,E.P. *et al*. (2002) Killing activity of neutrophils is mediated through activation of proteases by K^+ flux. *Nature*, **416**, 291–297.

Rotrosen,D. and Leto,T.L. (1990) Phosphorylation of neutrophil 47-kDa cytosolic oxidase factor. *J. Biol. Chem.*, **265**, 19910–19915.

Seguchi,H. and Kobayashi,T. (2002) Study of NADPH oxidase-activated sites in human neutrophils. *J. Electron Microsc.*, **51**, 87–91.

Stahelin,R.V. and Cho,W. (2001) Differential roles of ionic, aliphatic and aromatic residues in membrane–protein interactions: a surface plasmon resonance study on phospholipases A2. *Biochemistry*, **40**, 4672–4678.

Stahelin,R.V., Long,F., Diraviyam,K., Bruzik,K.S., Murray,D. and Cho,W. (2002) Phosphatidylinositol-3-phosphate induces the membrane penetration of the FYVE domains of Vps27p and Hrs. *J. Biol. Chem.*, **277**, 26379–26388.

Sumimoto,H., Kage,Y., Nunoi,H., Sasaki,H., Nose,T., Fukumaki,Y., Ohno,M., Minakami,S. and Takeshige,K. (1994) Role of Src homology 3 domains in assembly and activation of the phagocyte NADPH oxidase. *Proc. Natl Acad. Sci. USA*, **91**, 5345–5349.

Sumimoto,H., Hata,K., Mizuki,K., Ito,T., Kage,Y., Sakaki,Y., Fukumaki,Y., Nakamura,M. and Takeshige,K. (1996) Assembly and activation of the phagocyte NADPH oxidase—specific interaction of the N-terminal Src homology 3 domain of p47(phox) with p22(phox) is required for activation of the NADPH oxidase. *J. Biol. Chem.*, **271**, 22152–22158.

Swain,S.D., Helgerson,S.L., Davis,A.R., Nelson,L.K. and Quinn,M.T. (1997) Analysis of activation-induced conformational changes in

p47phox using tryptophan fluorescence spectroscopy. *J. Biol. Chem.*, **272**, 29502–29510.

Thomas,C.C., Dowler,S., Deak,M., Alessi,D.R. and van Aalten,D.M. (2001) Crystal structure of the phosphatidylinositol 3,4-bisphosphate-binding pleckstrin homology (PH) domain of tandem PH-domain-containing protein 1 (TAPP1): molecular basis of lipid specificity. *Biochem. J.*, **358**, 287–294.

Uhlinger,D.J., Tyagi,S.R., Inge,K.L. and Lambeth,J.D. (1993) The respiratory burst oxidase of human neutrophils. Guanine nucleotides and arachidonate regulate the assembly of a multicomponent complex in a semirecombinant cell-free system. *J. Biol. Chem.*, **268**, 8624–8631.

Wientjes,F.B., Reeves,E.P., Soskic,V., Furthmayr,H. and Segal,A.W. (2001) The NADPH oxidase components p47(phox) and p40(phox) bind to moesin through their PX domain. *Biochem. Biophys. Res. Commun.*, **289**, 382–388.

Yu,J.W. and Lemmon,M.A. (2001) All phox homology (PX) domains from *Saccharomyces cerevisiae* specifically recognize phosphatidylinositol 3-phosphate. *J. Biol. Chem.*, **276**, 44179–44184.

Zhan,Y., Virbasius,J.V., Song,X., Pomerleau,D.P. and Zhou,G.W. (2002) The p40phox and p47phox PX domains of NADPH oxidase target cell membranes via direct and indirect recruitment by phosphoinositides. *J. Biol. Chem.*, **277**, 4512–4518.

Received June 18, 2002; revised and accepted August 13, 2002